Thin Solid Films 706 (2020) 137984

Contents lists available at ScienceDirect

Thin Solid Films

journal homepage: www.elsevier.com/locate/tsf

Perfecting the dispersion model free characterization of a thin film on a substrate specimen from its normal incidence interference transmittance spectrum

D.A. Minkov[a,*], G.V. Angelov[b], R.N. Nestorov[b], E. Marquez[c]

[a] College of Energy and Electronics, Technical University, Sofia, 2140 Botevgrad, Bulgaria
[b] Department of Microelectronics, Faculty of Electronics Engineering and Technologies, Technical University, Sofia 1000, Bulgaria
[c] Faculty of Science, Department of Condensed-Matter Physics, University of Cadiz, 11510 Puerto Real, Cadiz, Spain

ARTICLE INFO

Keywords:
thin films
perfecting the characterization
dispersion model free
partially coherent light
light scattering
surface roughness.

ABSTRACT

An algorithm is proposed for perfecting the envelope method (EM) for characterization of a thin film on a substrate specimen from its normal incidence interference transmittance spectrum $T(\lambda)$. It takes into account the partial coherence of light propagating through the film, due to light scattering mainly associated with roughness of the surface film/air, in the computations of both the smoothed transmittance spectrum $T_{sm}(\lambda)$ and the extinction coefficient $k(\lambda)$ of the film. The algorithm includes enhanced computation of the envelopes $T_+(\lambda)$ and $T_-(\lambda)$ of $T_{sm}(\lambda)$, and adjustment of points $T_+(\lambda_t)$ and $T_-(\lambda_t)$ in spectral regions of substrate non-transparency as λ_t are the wavelengths of the tangency points between $T_{sm}(\lambda)$ and its envelopes. The average thickness $\bar{d}$ and the non-uniformity Δd of the film are computed by EM based optimization procedure, followed by obtaining the refractive index $n(\lambda)$ of the film by optimized curve fitting over approximated values $n_0(\lambda_t)$ of $n(\lambda_t)$ without employing a dispersion model. It is demonstrated that $k(\lambda)$ is determined more accurately from $T_{sm}(\lambda)$, based on computing its coherent light approximation $k_0(\lambda)$ and partially coherent light correction $\Delta k(\lambda)$, rather than the commonly used computation of $k(\lambda)$ from $T_+(\lambda)$. Two a-Si films with dissimilar thicknesses are characterized by the proposed algorithm; as there are published characterization results for the same films computed by two spectroscopic ellipsometry related methods, and two EMs, selected as most likely to provide accurate characterization of the films. Comparing the characterization accuracy for the proposed algorithm with the characterization accuracy for the best of these published results shows that using the proposed algorithm leads to significantly more accurate characterization of both a-Si films. Accurate characterization is achieved even in a case of $T(\lambda)$ influenced by residual gas absorption during its measurement, by employing both $T_{sm}(\lambda)$ and $T_+(\lambda)$ in the computation of $k(\lambda)$. The presented results indicate that using the proposed algorithm has a capacity for providing most accurate characterization of almost every dielectric or semiconductor film with $\bar{d}$ = [300,5000] nm on a substrate, only from $T(\lambda)$, compared to all the other methods for characterization of such films only from $T(\lambda)$.

1. Introduction

Specimens of a thin film on a substrate are widely used for optical characterization of the film. A sketch of such specimen and its main optical characteristics is shown in Fig. 1a. The normal incidence transmittance spectrum $T(\lambda)$, in the UV/VIS/NIR spectral region of wavelengths λ, of a thin dielectric or semiconductor film, with average thickness $\bar{d}$ = [300,5000] nm, on a glass substrate usually contains interference pattern with several maxima and minima [1,2]. A fundamental tool for film characterization from such $T(\lambda)$ is the envelope method (EM), which is a dispersion model free method since it does not employ any dispersion model. The EM uses computed upper envelope $T_+(\lambda)$ and lower envelope $T_-(\lambda)$ of the smoothed transmittance spectrum $T_{sm}(\lambda)$ of the noisy $T(\lambda)$. The tangency wavelengths $\lambda_t(i)$ represent the tangency points $T_{sm}(\lambda_t)$ between the two envelopes and $T_{sm}(\lambda)$, where ´i´ is a positive integer showing the number of the ´i-th´ extremum of $T_{sm}(\lambda)$ counted from 1 closest from the higher wavelengths end.

The EM using only $T(\lambda)$ has three main versions: the founding EM (FEM) of Swanepoel [3] with over 4000 citations, the improved EM

* Corresponding author.
E-mail address: d.minkov@tu-sofia.bg (D.A. Minkov).

https://doi.org/10.1016/j.tsf.2020.137984
Received 20 September 2019; Received in revised form 24 March 2020; Accepted 25 March 2020
Available online 12 May 2020

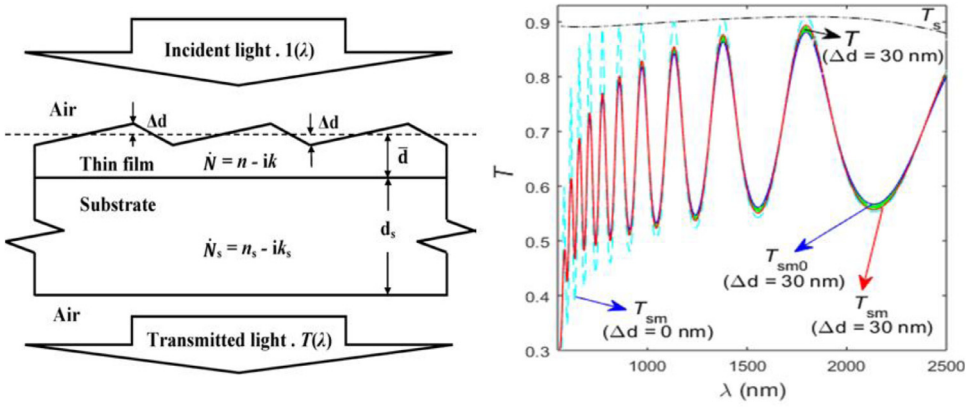

Figure 1. a) A sketch of a thin film on a substrate specimen, and its main optical characteristics. b) $T(\lambda)$ and $T_{sm}(\lambda)$ for a model specimen of a-Si:H film with $n = 3 \times 10^5/\lambda^2 + 2.6$, $k = [\lambda/(4\pi)]\cdot 10^{(1.5\times 10^6/\lambda^2)-8}$, and $\bar{d} = 1000$ nm, on a 0.9 mm thick Corning7059 glass substrate [5]. $T_{sm}(\lambda)$ of the specimen is computed from Eq. (1) for an uniform film (with $\Delta d = 0$), and for a non-uniform film with $\Delta d = 30$ nm. Augmentedly noisy $T(\lambda)$, in green, and its ordinary 'internally smoothed' T_{sm0}(internal) are illustrated for the specimen with $\Delta d = 30$ nm. T_s is the transmittance through the substrate without a film.

(IEM) [4], and the optimizing EM (OEM) [5]. In [3], and its modifications [6–11] is considered the simplest case of a film with uniform thickness. Unlike the FEM and IEM, the OEM selects optimized values of $\bar{d}$ and the non-uniformity $\Delta d \geq 0$ of the film thickness, as Δd represents the maximum deviation of the film thickness from $\bar{d}$ over the light spot on the surface film/air. It was demonstrated in [5,12] that the OEM provides more accurate film characterization compared to the FEM and IEM.

Every EM version is based on a formula for $T_{sm}(\lambda)$, and an interference fringes equation referring to each $\lambda_t(i)$. The most accurate formula for $T_{sm}(\lambda)$ is used in [5], and is rewritten as:

$$T_{sm}(\lambda) = \frac{1}{\varphi_2 - \varphi_1}\int_{\varphi_1}^{\varphi_2} dT_u(\varphi) = \frac{(\tau_{a,f}\tau_{f,s}\tau_{s,a})^2 x_s}{\varphi_2 - \varphi_1}\int_{\varphi_1}^{\varphi_2}\frac{x d\varphi}{a_1 - b_1\cos(\varphi) + c_1\sin(\varphi)}, \quad (1)$$

where $\varphi = 4\pi n d/\lambda$, $\varphi_1 = 4\pi n(\bar{d} - \Delta d)/\lambda$, $\varphi_2 = 4\pi n(\bar{d} + \Delta d)/\lambda$,

$a_1 = 1 - x(\rho_{a,f}\rho_{s,a}x_s)^2 + \rho_{f,s}^2(x_s - x + \rho_{s,a}^2 x_s^3)$,

$b_1 = 2\rho_{a,f}\rho_{f,s}\rho_{s,a}x[\rho_{s,a}x_s^2\cos\Delta_2 - \rho_{s,a}^{-1}\cos\Delta_1]$,

$c_1 = 2\rho_{a,f}\rho_{f,s}\rho_{s,a}x[\rho_{s,a}x_s^2\sin\Delta_2 - \rho_{s,a}^{-1}\sin\Delta_1]$,

$$\tau_{a,f}\tau_{f,s}\tau_{s,a} = \frac{8}{\sqrt{(n+1)^2 + k^2}}\sqrt{\frac{n^2 + k^2}{(n + n_s)^2 + (k + k_s)^2}}\sqrt{\frac{n_s^2 + k_s^2}{(n_s+1)^2 + k_s^2}},$$

$$\rho_{a,f} = \sqrt{\frac{(n-1)^2 + k^2}{(n+1)^2 + k^2}}, \quad \rho_{f,s} = \sqrt{\frac{(n - n_s)^2 + (k - k_s)^2}{(n + n_s)^2 + (k + k_s)^2}},$$

$$\rho_{s,a} = \sqrt{\frac{(n_s - 1)^2 + k_s^2}{(n_s + 1)^2 + k_s^2}},$$

$$\Delta_1 = \tan^{-1}\left(\frac{2k}{n^2 + k^2 - 1}\right) + \pi + \tan^{-1}\left[\frac{2(kn_s - k_s n)}{n^2 - n_s^2 + k^2 - k_s^2}\right],$$

$$\Delta_2 = \tan^{-1}\left(\frac{2k}{n^2 + k^2 - 1}\right) + \pi - \tan^{-1}\left[\frac{2(kn_s - k_s n)}{n^2 - n_s^2 + k^2 - k_s^2}\right];$$

$T_u(\lambda)$ represents the transmittance of an uniform film, $n(\lambda)$, $k(\lambda)$, and $x(\lambda)$ are the refractive index, the extinction coefficient, and the absorbance of the film, and the subscript 's' refers to the respective known substrate characteristics. It is assumed in Eq. (1) that the film thickness d has a continuous uniform distribution in the interval $[\bar{d} - \Delta d, \bar{d} + \Delta d]$ over the light spot on the film surface, and any light scattering from the film is ignored. However, Eq. (1) can be modified and used for any known distribution of d over the light spot.

The interference fringes equation is:

$$2n(\lambda_t)\bar{d} = m_i(\lambda_t)\lambda_t(i) \begin{cases} m_i \geq 1 - \textit{integer for all tangency wavelengths } \lambda_{t+} \\ \quad \textit{from the envelope } T_+(\lambda) \\ m_i \geq 1/2 - \\ \quad \textit{half} - \textit{integer for all tangency wavelengths } \lambda_{t-} \\ \quad \textit{from the envelope } T_-(\lambda). \end{cases} \quad (2)$$

The use of Eq. (2) in addition to Eq. (1) can result in more accurate film characterization by the EM compared to film characterizations by methods not using interference fringes equation [12,13].

In all of the three main EM versions [3–5] is used ordinary 'internal smoothing' [12,14] of the inherently noisy $T(\lambda)$, leading to $T_{sm0}(\lambda)$ passing slightly below the peaks and above the valleys of $T(\lambda)$, therefore slightly shrinking the interference pattern as illustrated in Fig. 1b. Correspondingly, it was indicated in [12] that employing 'external smoothing', which provides $T_{sm}(\lambda)$ passing slightly externally to $T(\lambda)$ in the regions around its extrema and also illustrated in Fig. 1b, can increase the film characterization accuracy when using the OEM, compared with 'internal smoothing' of $T(\lambda)$.

Regarding the computation of the envelopes $T_+(\lambda)$ and $T_-(\lambda)$ of $T_{sm}(\lambda)$, the following approximation was derived for a film on a glass substrate in the spectral region of weak film absorption and small variation of $n(\lambda)$ [15]:

$$\frac{1}{x_s(E)}\frac{dT_\pm(E)}{dE} \cong const_\pm \leq 0, \quad where\ E(eV) = 1239.8/\lambda(nm)\ is\ the\ photon\ energy, \quad (3)$$

as '+' from the ' ± ' sign refers to $T_+(E)$ and '−' refers to $T_-(E)$. With respect to the longest wavelength λ_L of $T(\lambda)$, in the spectral region of weak film absorption and small variation of $n(\lambda)$, using finite difference representation of the derivative in Eq. (3) provides:

$$T_\pm(\lambda_L) \cong x_s(\lambda_L)\left\{\frac{T_\pm(\lambda_{t1\pm})}{x_s(\lambda_{t1\pm})} + \left[\frac{T_\pm(\lambda_{t1\pm})}{x_s(\lambda_{t1\pm})} - \frac{T_\pm(\lambda_{t2\pm})}{x_s(\lambda_{t2\pm})}\right]\frac{(\lambda_L - \lambda_{t1\pm})\lambda_{t2\pm}}{(\lambda_{t1\pm} - \lambda_{t2\pm})\lambda_L}\right\}, \quad (4)$$

where '+' from the ' ± ' signs refers to $T_+(\lambda)$ and '−' to $T_-(\lambda)$, as $\lambda_{t1\pm}$and $\lambda_{t2\pm} < \lambda_{t1\pm}$ are the two longest tangency wavelengths from $T_+(\lambda)$ or $T_-(\lambda)$ [16]. Eq. (4) can introduce right 'boundary points' for $T_+(\lambda)$ and $T_-(\lambda)$.

There are two main algorithms for computation of the envelopes

$T_+(\lambda)$ and $T_-(\lambda)$, for a thin film on a glass substrate specimen, presented in [16] and [17]. The algorithm from [16] uses left and right 'boundary points', 'additional points', and 'supplementary points', for each of the envelopes $T_+(\lambda)$ and $T_-(\lambda)$, without employing iteration. The algorithm from [17] uses iteration, for each of the envelopes, without including any of the above extra points. However, both algorithms from [16] and [17] assume transparent substrate or a self supporting film, i.e. $x_s(\lambda) = 1$, except for the computation of the right 'boundary points' in [16]; although commonly used glass substrates absorb considerably for $\lambda > 2000$ nm, whereas $x_s(\lambda > 2000\ \text{nm}) < 1$ [18]. Furthermore, there is an approach for increasing the accuracy of computation of $T_+(\lambda)$ and $T_-(\lambda)$, especially in the strong absorption region, by using a "rectifying process", accounting for the decreased accuracy in cases of smaller number of interference fringes [19]. Notably, the use of the OEM from [5] alleviates the problem of envelopes inaccuracy in the strong absorption region by computation of $\bar{d}$ and Δd of the film, automatically disregarding the data from this region.

Since $T_{sm}(\lambda) \sim x_s(\lambda) \leq 1$ according to Eq. (1), the envelopes of $T_{sm}(\lambda)$ should obey the relations $T_+(\lambda) \sim x_s(\lambda)$ and $T_-(\lambda) \sim x_s(\lambda)$, i.e. they should be proportional to the substrate absorbance $x_s(\lambda)$. Because of this, employing 'adjusted for $x_s(\lambda) \leq 1$ envelopes' $T_+(\lambda)$ and $T_-(\lambda)$ computed by modifying 'conventional envelopes' of $T_{sm}(\lambda)$, obtained assuming $x_s(\lambda) = 1$, was proposed in [12].

The formula providing most accurate approximation of $T_+(\lambda_t)$ and $T_-(\lambda_t)$ is [5]:

$$T_{\pm}(\lambda_t) \cong \frac{(\tau_{a,f_0}\tau_{f,s_0}\tau_{s,a_0})^2\bar{x}x_s}{\theta\sqrt{{a_{1_0}}^2 - {b_{1_0}}^2}}\text{atan2}\left[\frac{a_{1_0} \pm b_{1_0}}{\sqrt{{a_{1_0}}^2 - {b_{1_0}}^2}}\tan(\theta)\right], \tag{5}$$

where ´+´ from the ´ ± ´ signs refers to $T_+(\lambda)$, and ´-´ to $T_-(\lambda)$,

$$\theta = 2\pi n\Delta d/\lambda_t,\ \ \bar{x} = \exp(-4\pi k\bar{d}/\lambda_t),$$

$$a_{1_0} = 1 - \left(\rho_{a,f_0}\rho_{s,a_0}\bar{x}x_s\right)^2 + {\rho_{f,s_0}}^2\left({\rho_{a,f_0}}^2\bar{x}^2 - {\rho_{s,a_0}}^2{x_s}^2\right),$$

$$b_{1_0} = 2\rho_{a,f_0}\rho_{f,s_0}\rho_{s,a_0}\bar{x}\left({\rho_{s,a_0}}^{-1} - \rho_{s,a_0}{x_s}^2\right),$$

$$\tau_{a,f_0} = \frac{2}{n+1},\ \ \tau_{f,s_0} = \frac{2n}{n+n_s},\ \ \tau_{s,a_0} = \frac{2n_s}{n_s+1},\ \ \rho_{a,f_0} = \frac{n-1}{n+1},$$
$$\rho_{f,s_0} = \frac{n-n_s}{n+n_s},\ \ \rho_{s,a_0} = \frac{n_s-1}{n_s+1}.$$

In fact, Eq. (5) is also valid for every λ, thus it can be used for formulation of both envelopes $T_+(\lambda)$ and $T_-(\lambda)$. Notably, (1,2,5) have been derived assuming $n^2(\lambda) > {n_s}^2(\lambda) >> k^2(\lambda)$ and ${n_s}^2(\lambda) >> {k_s}^2(\lambda)$ [4], whereas these relationships are commonly satisfied, in the UV/VIS/NIR spectral region, for a thin dielectric or semiconductor film with $\bar{d}$ = [300,5000] nm on a glass substrate [9]. Replacing the above inequalities in the formulae for a_1, b_1 and c_1 from Eq. (1) leads to $a_1 > b_1 > 0$ and $b_1 >> |c_1|$. In (5), the function $-\pi < \text{atan2}(.) \leq \pi$ represents $-\pi/2 < \tan^{-1}(u_n/u_d) \leq \pi/2$, in computations, for unambiguous description of the phase change π of reflected light when it falls from a lower refractive index medium [15].

Each film characterization by the EM is executed in two stages. In the first stage of FEM characterization are computed the thickness d of the film assumed to be uniform, and the consecutive positive integer and half-integer interference orders $m_i[\lambda_t(i)]$ [3]. In the first stage of IEM or OEM characterization are computed the average film thickness $\bar{d}$, the non-uniformity Δd of the film thickness, and $m_i[\lambda_t(i)]$ [4,5]. Furthermore, in first stage OEM characterization, the set $\{\bar{d},\Delta d,m_1\}$ is optimized to provide smallest value of the error metric:

$$SD/N = \frac{\sqrt{\frac{\sum_{i=1}^{N}[\bar{d} - \bar{d}_0[\lambda_t(i)]]^2}{N}}}{N}\ \ or\ \ RMSD/N = \frac{\sqrt{\frac{\sum_{i=1}^{N}\{m_i[\lambda_t(i)] - m_{i_0}[\lambda_t(i)]\}^2}{N}}}{N}, \tag{6}$$

where $m_{i_0}[\lambda_t(i)]$ are estimated real number values of $m_i[\lambda_t(i)]$, $\bar{d}_0[\lambda_t(i)]$ are estimated values of $\bar{d}$, and N is an optimized number of adjacent tangency wavelengths $\lambda_t(i)$ participating in these computations [5,12]. The employment of larger optimized N in the error metric from Eq. 6 and more accurate optimized values of $\bar{d}$ and m_1 make possible accurate characterization of thicker films by the OEM in comparison with the FEM and the IEM [5,12]. In general, relatively high accuracy of computation of $\bar{d}$, Δd, and m_i can be achieved in the EM as a result of coordinated use of $T_\pm(\lambda_t)$ and Eq. (2) for several λ_t, averaging, and iteration [3–5,12].

The second stage of EM characterization starts by calculation of the refractive index $n(\lambda_t)$ of the film for each $\lambda_t(i)$ from Eq. (2) [3–5,12]. The extinction coefficient $k(\lambda_t)$ of the film is commonly computed from the approximation of $T_+(\lambda_t)$ e.g. by solution of Eq. (5) for each $\lambda_t(i)$ [3–5,20]. Alternatively, $k(\lambda_t)$ can be computed from $T_{sm}(\lambda_t)$ by numerical integration and solution of Eq. (1) for each $\lambda_t(i)$ [12]. Approximations of $n(\lambda)$ and $k(\lambda)$ can be derived e.g. by interpolations over $n(\lambda_t)$ and $k(\lambda_t)$, respectively [4,12]. In fact, the optimization of the set $\{\bar{d},\Delta d,m_1\}$ at the first stage of OEM characterization is the main distinction of the OEM from the IEM, as the second stages of OEM and IEM characterizations are similar [4,5,12].

Replacing the computed $\bar{d}$, Δd, $n(\lambda)$ and $k(\lambda)$ in the right side of Eq. (1), executing the numerical integration, provides a reconstructed transmittance spectrum $T_r(\lambda)$. A figure of merit *FOM* of a particular EM film characterization was defined in [12] as the root mean square deviation of $T_r(\lambda)$ from $T(\lambda)$, with summation over all $\lambda \subset [\min(\lambda_t),\lambda_t(1)]$:

$$FOM = \sqrt{\frac{\sum_{j=1}^{N_j}\{T[\lambda(j)] - T_r[\lambda(j)]\}^2}{N_j}}, \tag{7}$$

where Nj is the total number of such wavelengths. Therefore, for a given specimen, the film characterization providing smallest *FOM* is considered as the most accurate characterization over the wavelengths interval $[\min(\lambda_t),\lambda_t(1)]$ since its respective $T_r(\lambda)$ fits best the experimental spectrum $T(\lambda)$.

Since a-Si films are usually assumed to have Urbach tails [21,22], the *FOM*s were compared in [12] for characterizations of two radio frequency (RF) magnetron sputtered a-Si thin films with dissimilar average thicknesses by the OEM, the optimizing graphical method (OGM) [23], the Tauc-Lorentz-Urbach model method (TLUM) [24], and the Cody-Lorentz-Urbach model method (CLUM) [25]. In [12], the OEM and OGM computed $n(\lambda)$ and $k(\lambda)$ mainly by ´piecewise cubic Hermite polynomial interpolation´ (PCHPI) [26] over $n(\lambda_t)$ and $k(\lambda_t)$, respectively. The results from [12] showed that the OEM provided most accurate characterization, of both films, among the four different characterization methods. The superior performance of the OEM was explained considering that it does not assume particular band tails shapes, unlike the TLUM and CLUM; and it does not assume existence of a wide spectral region of film transparency as an initial approximation, unlike the OGM [12].

However, there are three important factors hampering further accuracy improvement of film characterization based on the OEM, commented next in the order of appearance in the film characterization process. The first factor is the incapability to compute accurate 'adjusted for $x_s(\lambda) \leq 1$ envelopes' $T+(\lambda)$ and $T-(\lambda)$, since the main algorithms for computation of the envelopes [16,17] do not employ either iteration or extra envelope points and do not account accurately for $x_s(\lambda) \leq 1$. The second factor originates from the fact that inevitable inaccuracies of $T_{sm}(\lambda)$ result in errors in some tangency wavelengths $\lambda_t(i)$, and in the respective $n[\lambda_t(i)]$ calculated from Eq. (2). In this regard, deriving $n(\lambda)$ and $k(\lambda)$ by interpolations over $n(\lambda_t)$ and its respective $k(\lambda_t)$ leads to appearance of spurious small humps in both $n(\lambda)$ and $k(\lambda)$ [12]. The third factor originates from the possibility of significant relative errors in the computation of $k(\lambda_t)$ due to inaccuracy of $T_+(\lambda_t)$ or $T_{sm}(\lambda_t)$, small values of $k(\lambda_t) << n(\lambda_t)$ for $\lambda_t \subset [\min(\lambda_t),\lambda_t(1)]$, and inaccuracy of $n(\lambda_t)$ [12,27]. This can lead to large errors in $k(\lambda)$

interpolated over the strongly non-linear dependence $k(\lambda_t)$.

In this paper is proposed an algorithm for perfecting the EM characterization of a thin film on glass substrate specimen, from its normal incidence interference transmittance spectrum $T(\lambda)$, by diminishing the influence of the above three factors limiting the accuracy of characterization. The algorithm described in the next section is used for characterization of the two a-Si films with dissimilar thicknesses, from the respective specimens A038 and A041, already OEM characterized in [12]. These films have been deposited by RF magnetron sputtering using applied RF power of 525 W, target-to-substrate distance of 6.1 cm, and Ar gas. The film from A038 has been deposited on 0.9 mm thick Corning7059 glass substrate, with Ar pressure of 4.4 Pa; and the film from A041 - on 3.28 mm thick Borofloat33 glass substrate, with Ar pressure of 0.13 Pa. The area of the light spot on the film surface has been 10 mm × 3 mm in the measurements of $T(\lambda)$ of A038 and A041.

Notably, these films are challenging for accurate characterization. Indeed, the film from A038 is quite thin which leads to too small number of extrema of its respective $T_{sm}(\lambda)$, and possible errors in the computation of accurate envelopes and tangency wavelengths λ_t; as the film from A041 is quite thick which tends to cause errors in the computations of $T_{sm}(\lambda)$ and the first interference order m_1. Furthermore, both specimens A038 and A041 have tangency points $T_{sm}(\lambda_t)$ within the apparent spectral region of non-transparency of the substrate, which necessitates correcting the locations of at least several points from the 'conventional envelopes' of $T_{sm}(\lambda)$ to adjust for $x_s(\lambda) < 1$.

2. Description of the algorithm for perfecting the EM characterization of a thin film on glass substrate specimen from its normal incidence interference transmittance spectrum $T(\lambda)$

The proposed algorithm is presented in Fig. 2, and its steps are commented below.

Step A1. Importantly, Eq. (1) regards the light propagating through the film as coherent. However, the light propagating through the film is partially coherent, due to the finite slit width of the source [3] and the light scattering from the film [28,29]. Furthermore, the partial coherence of light due to scattering has not been considered in dispersion model free characterization of a film. In this regard, propagation of partially coherent light through the film should result in shrinkage of the interference pattern, since $b_1 >> |c_1|$ and contributions from different phase differences φ disallow the average $\overline{\cos(\varphi)}$ to reach ± 1 in Eq. (1). In other words, the thin film interference from uniform film with a thickness $d \subset [\bar{d}-\Delta d, \bar{d}+\Delta d]$ creates the interference pattern in $T(\lambda)$; as the scattering from the film, and the finite slit width, slightly shrink the interference pattern, as illustrated in Fig. 1b. To account for these effects, an 'internal smoothing' of $T(\lambda)$ is performed, leading to $T_{sm0}(\lambda)$, followed by 'external smoothing' of $T(\lambda)$, which furnishes $T_{sm1}(\lambda)$ and represents a correction for the partial coherence of light due to the scattering. $T_{sm1}(\lambda)$ is then corrected for the finite slit width, using the slit width correction from [3,5], which provides $T_{sm}(\lambda)$. Such $T_{sm}(\lambda)$ corresponds to propagation of coherent light through the film, and is compatible with Eq. (1) and Eq. (2) which also assume propagation of coherent light through the film.

Based on the above, the computed by 'external smoothing' spectrum $T_{sm1}(\lambda)$ touches externally $T(\lambda)$ in the regions around its extrema as discussed in the Introduction. The smoothed transmittance spectrum $T_{sm}(\lambda)$ is obtained by a slit width correction of $T_{sm1}(\lambda)$ as described in [12]. For the specimens A038 and A041, $|T_{sm}(\lambda)-T_{sm1}(\lambda)| \subset [0.0005,0.004]$.

Step A2. The envelope $T_+(\lambda)$ is computed by iteration decreasing to zero the sum

$S_+^{(l)} = \sum_{i=1}^{N_+} |T_{sm}[\Lambda_+^{(l)}(i)] - T_+^{(l)}[\Lambda_+^{(l)}(i)]|$, where l is the iteration step number, N_+ is the number of maxima of $T_{sm}(\lambda)$ plus the number of 'additional points' for $T_+(\lambda)$, and the approximated wavelengths set$\{\Lambda_+^{(l)}(i)\} = \{\lambda_{t_+}^{(l)}, \lambda_{a_+}^{(l)}\}$ consists of $\lambda_{t_+}^{(l)}$ for the tangency points and $\lambda_{a_+}^{(l)}$for the 'additional points' for $T_+(\lambda)$ used at step l. $T_+^{(l)}(\lambda)$ is an approximation of $T_+(\lambda)$ obtained by PCHPI over the points corresponding to $\{\Lambda_+^{(l)}(i)\}$, the 'supplementary points', and the 'boundary points' for $T_+(\lambda)$ at step l; whereas the right 'boundary point' $T_+^{(l)}(\lambda_L)$ is computed from Eq. (4) and depends on l. At the end of step l is determined the set $\{\Lambda_+^{(l+1)}(i)\}$, to be used at the iteration step $l+1$, consisting of the wavelengths corresponding to the maxima of the function $T_{sm}(\lambda) - T_+^{(l)}(\lambda)$. The envelope $T_-(\lambda)$ is computed similarly to $T_+(\lambda)$, by iteration decreasing to zero the sum $S_-^{(l)} = \sum_{i=1}^{N_-} |T_-^{(l)}[\Lambda_-^{(l)}(i)] - T_{sm}[\Lambda_-^{(l)}(i)]|$, where N_- is the number of minima of $T_{sm}(\lambda)$ plus the number of 'additional points' for $T_-(\lambda)$. The set $\{\Lambda_-^{(l+1)}(i)\}$ to be used at the iteration step $l+1$ consists of the wavelengths corresponding to the maxima of the function $T_-^{(l)}(\lambda) - T_{sm}(\lambda)$. Since the envelopes should only touch $T_{sm1}(\lambda)$, without crossing it, the iteration for computing $T_+(\lambda)$ should always finish with $S_+^{(l)} = 0$, and the iteration for computing $T_-(\lambda)$ should always finish with $S_-^{(l)} = 0$. It usually takes 2 to 4 steps to complete each of these two iterations.

Step A3. The tangency wavelengths $\lambda_{t_+} = \lambda_{t_+}^{(l)}$ and their respective envelope $T_+(\lambda) = T_+^{(l)}(\lambda)$ are taken from the iteration step providing

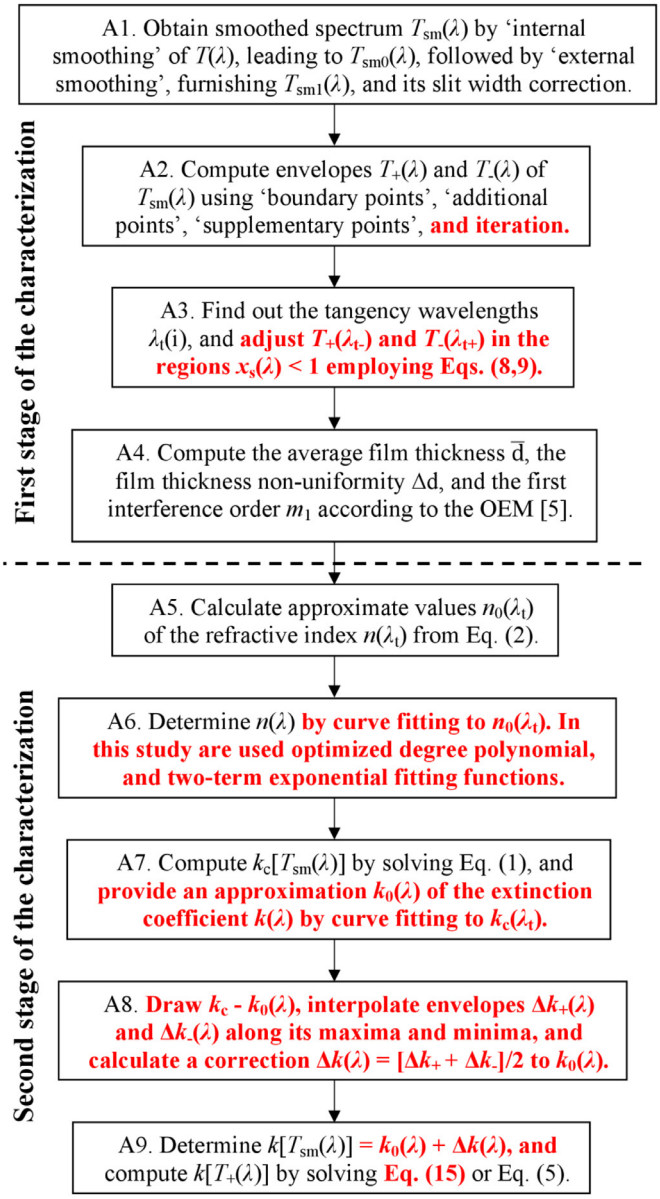

Figure. 2. The algorithm for perfecting the EM characterization of a thin film on glass substrate. The original elements of this algorithm, compared to the algorithms used in [5,12], are shown in red.

$S_+^{(l)} = 0$, while the tangency wavelengths $\lambda_{t\_} = \lambda_{t\_}^{(l)}$ and their respective envelope $T_-(\lambda) = T_-^{(l)}(\lambda)$ are taken from the iteration step providing $S_-^{(l)} = 0$. Besides, in the computation of the envelopes $T_+(\lambda)$ and $T_-(\lambda)$, obtained from step A2, is assumed implicitly $x_s(\lambda) = 1$, although commonly used glass substrates absorb significantly for $\lambda >$ 2000 nm and $x_s(\lambda > 2000\ \text{nm}) < 1$ [18]. Moreover, $T_+(\lambda_{t\_})$ and $T_-(\lambda_{t+})$ are used in the first stages of each main EM version [3–5], and they do not belong to $T_{sm}(\lambda)$. Consequently, proper adjusting their values for $x_s(\lambda) \le 1$ should lead to more accurate film characterization.

Adjusted $T_+(\lambda_{t\_})$ and $T_-(\lambda_{t+})$ in regions with $x_s(\lambda) < 1$ are formulated similarly to the expression from Eq. (4) by using finite difference representation of the derivative in Eq. (3), whereas:

$$T_{\pm}[\lambda_{t\mp}(i)] \cong x_s[\lambda_{t\mp}(i)]\left(\frac{T_{\pm}[\lambda_{t\pm}(i-1)]}{x_s[\lambda_{t\pm}(i-1)]} + \left\{\frac{T_{\pm}[\lambda_{t\pm}(i-1)]}{x_s[\lambda_{t\pm}(i-1)]} - \frac{T_{\pm}[\lambda_{t\pm}(i+1)]}{x_s[\lambda_{t\pm}(i+1)]}\right\} \frac{[\lambda_{t\mp}(i) - \lambda_{t\pm}(i-1)]\lambda_{t\pm}(i+1)}{[\lambda_{t\pm}(i-1) - \lambda_{t\pm}(i+1)]\lambda_{t\mp}(i)}\right). \tag{8}$$

For the only one still unchanged either $T_+[\lambda_{t\_}(1)]$ or $T_-[\lambda_{t+}(1)]$, its adjusted value in a region with $x_s(\lambda) < 1$ is formulated, based on Eq. (4) and Eq. (8), as:

$$T_{\pm}[\lambda_{t\mp}(1)] \cong x_s[\lambda_{t\mp}(1)]\left\{\frac{T_{\pm}(\lambda_{t1\pm})}{x_s(\lambda_{t1\pm})} + \left[\frac{T_{\pm}(\lambda_{t1\pm})}{x_s(\lambda_{t1\pm})} - \frac{T_{\pm}(\lambda_{t2\pm})}{x_s(\lambda_{t2\pm})}\right] \frac{[\lambda_{t\mp}(1) - \lambda_{t1\pm}]\lambda_{t2\pm}}{(\lambda_{t1\pm} - \lambda_{t2\pm})\lambda_{t\mp}(1)}\right\}. \tag{9}$$

Since $x_s(\lambda) \cong 1$ in the regions of quasi-transparency of the substrate, $T_+(\lambda_{t\_})$ and $T_-(\lambda_{t+})$ are not adjusted for $x_s(\lambda) < 1$ in these regions.

Steps A4 and A5. In the beginning of this step are known the substrate characteristics $n_s(\lambda)$, $k_s(\lambda)$, and d_s; as well as $T_{sm}(\lambda)$, all $\lambda_t(i)$, $T_+(\lambda_t)$, and $T_+(\lambda_t)$. Considering the comments from the Introduction, optimized values of the average film thickness $\bar{d}$, the film thickness non-uniformity Δd, and the first interference order m_1 are computed according to the first stage film characterization by the OEM, as described in [5]. Approximate values $n_0(\lambda_t)$ of the refractive index $n(\lambda_t)$ are calculated thereafter from Eq. (2).

Step A6. Noticeably, $n(\lambda)$ should be a smooth function [1,24,25,30,31,32], and error can occur in $n_0(\lambda_t)$ for any particular tangency wavelength $\lambda_t(i)$. Therefore, based on statistical considerations [14], interpolation using $n_0(\lambda_t)$ can incur spurious small humps on $n(\lambda)$, however, curve fitting using $n_0(\lambda_t)$ can avoid occurrence of such humps and lead to more accurate EM characterization. Correspondingly, in this study is employed only curve fitting over $n_0\{\Lambda_f\}$ for obtaining $n(\lambda)$; whereas the wavelengths set $\{\Lambda_f\} = \{\lambda_t,\lambda_a\}$, with N_f elements, consists of all λ_t and λ_a for the 'additional point' with longest wavelength. λ_a is included in the set $\{\lambda_t,\lambda_a\}$ to ensure accurate curve fitting for $\lambda \approx \min(\lambda_t)$, since $n(\lambda)$ usually changes significantly for such short wavelengths.

Taking into account results about the optical constants of amorphous semiconductors [24,25], only the following two types of fitting functions *Ff* are used for curve fitting over $n_0\{\Lambda_f\}$ for the a-Si films from the specimens A038 and A041:

$$\begin{cases} 1).\ Ff = \textit{Polynomial of optimized degree } p_o \\ \qquad \le N_f - 1 \textit{ providing } \min[Fr(p)/(N_f - 1 - p)], \\ \textit{where:} \\ N_f - 1 \textit{ is the number of tangency wavelengths } \lambda_t, \\ p \textit{ is the polynomial degree}, \\ Fr(p) \\ \qquad \textit{is the sum of the square of the residuals over the set } \{ \\ \qquad \Lambda_f\} \textit{ for the polynomial of degree } p \text{ [33]}, \\ e.g.\ Fr(n\{\Lambda_f\}, p) = \sum_{f=1}^{N_f} [Ff(n\{\Lambda_f\}) - n_0\{\Lambda_f\}]^2; \ldots \\ 2).\ Ff = \textit{Two} - \textit{terms exponential} = u_1 \exp(u_2\lambda) \\ \qquad + u_3 \exp(u_4\lambda);\ u_1,\ u_2,\ u_3, \\ u_4 \textit{ are adjustable parameters.} \end{cases} \tag{10}$$

Using the two-terms exponential from (10) can provide a better fit over some dependences $n_0\{\Lambda_f\}$ which are too steep to be fitted well by polynomial functions [33]. The curve fitting over $n_0\{\Lambda_f\}$ at step A6 provides the refractive index $n(\lambda)$ of the film, as only the extinction coefficient $k(\lambda)$ of the film remains unknown.

Steps A7, A8 and A9. Computation of extinction coefficient $k(\lambda)$ of the film with low relative error is significantly more difficult than computation of accurate $n(\lambda)$, especially in the region $k(\lambda) << n(\lambda)$, as indicated in the penultimate paragraph of the Introduction. Furthermore, $k(\lambda)$ is usually computed in the EM based on solving equation for the envelope $T_+(\lambda)$ for each λ_t [3–5], rather than on using $T_{sm}(\lambda)$. However, besides the possible inaccurate computation of $T_+(\lambda_t)$, the partial coherence of light due to scattering, can influence notably $T_+(\lambda_t)$ as explained in the discussion about Step A1. These two factors can result in inaccurate computation of $k(\lambda)$ from equation for the envelope $T_+(\lambda)$, which considers the light propagating through the film as coherent, such as Eq. [5]. Since $T_{sm}(\lambda)$ is computed more accurately in its regions away from λ_t, and $T_{sm}(\lambda)$ is influenced less by the partial coherence of light in the same regions away from λ_t, as indicated regarding Step 1, it is reasonable to use $T_{sm}(\lambda)$ for accurate computation of $k(\lambda)$.

The problem with using Eq. (1) for determination of the extinction coefficient is that the respectively computed $k_c[T_{sm}(\lambda)]$ usually contains spurious small humps due to small inaccuracies of $T_{sm}(\lambda)$, the partial coherence of light, the small values of $k(\lambda_t) << n(\lambda_t)$, and small inaccuracy of $n(\lambda_t)$. Nevertheless, $k_c(\lambda_t)$ represents a rough estimate of $k(\lambda_t)$ although error can occur in $k_c(\lambda_t)$ for any particular $\lambda_t(i)$. Since $k(\lambda)$ should be a smooth function [1,24,25,30–32], interpolation using $k_c(\lambda_t)$ can incur small humps on $k(\lambda)$; however, curve fitting using $k_c(\lambda_t)$ can avoid occurrence of such humps and lead to more accurate EM characterization. Correspondingly, in this study of $k(\lambda)$ is employed only curve fitting over $k_c\{\Lambda_f\} = k_c\{\lambda_t,\lambda_a\}$; whereas only the fitting functions *Ff* from Eq. (10) are used for such curve fitting, which provides an approximation $k_0(\lambda)$ of $k(\lambda)$. Notably, since $k_c(\lambda_t)$ and $k_0(\lambda)$ are obtained based on using Eq. (1), which is valid for coherent light propagating through the film, $k_0(\lambda)$ represents a coherent light approximation of $k(\lambda)$.

Furthermore, the area $S_{coh}(\chi \subset [\chi_i = 4\pi n\bar{d}/\lambda_t(i), \chi_{i+1} = 4\pi n\bar{d}/\lambda_t(i+1)])$, between the interval $[\chi_i,\chi_{i+1}]$ and the segment $T_u([\chi_i,\chi_{i+1}])$ of the interference transmittance spectrum of a specimen with constant film thickness, is approximated by using Eq. (1) as:

$$S_{coh}([\chi_i, \chi_{i+1}]) = \int_{\chi_i}^{\chi_{i+1}} T_u(\chi)\mathrm{d}\chi = \int_{2\pi m_i}^{2\pi(m_i+1/2)} T_u(\chi)\mathrm{d}\chi \xrightarrow{c_1 \ll a_1+b_1} \frac{\pi(\tau_{a,f}\tau_{f,s}\tau_{s,a})^2 x_s x}{\sqrt{a_1^2 - b_1^2}},$$
$$where\ \ \chi = 4\pi n\bar{\mathrm{d}}/\lambda, \tag{11}$$

since $a_1 > b_1 >> |c_1|$, assuming propagation of coherent light through the film, and constant values of $n(\lambda)$ and $k(\lambda)$ over the interval $\lambda \subset [\lambda_t(i),\lambda_t(i+1)]$.

The respective area $S_{inc}(\chi \subset [\chi_i,\chi_{i+1}])$ of the interference free transmittance spectrum of a specimen with constant film thickness is approximated as:

$$S_{inc}([\chi_i, \chi_{i+1}]) = \int_{\chi_i}^{\chi_{i+1}} \left[\int_{\chi_i}^{\chi_{i+1}} \frac{T_u(\chi)}{\chi_{i+1} - \chi_i} d\chi \right] d\chi \xrightarrow{c_1 \ll a_1+b_1} \frac{\pi(\tau_{a,f}\tau_{f,s}\tau_{s,a})^2 x_s x}{\sqrt{a_1^2 - b_1^2}}, \tag{12}$$

assuming propagation of incoherent light through the film, and constant $n(\lambda)$ and $k(\lambda)$ over the interval $\lambda \subset [\lambda_t(i),\lambda_t(i+1)]$, in accordance with [34]. Since the approximation $c_1 << a_1 + b_1$ is usually satisfied for a thin dielectric or semiconductor film with $\bar{\mathrm{d}}$ = [300,5000] nm on a glass substrate [5,12], Eqs. (11,12) show that $S_{coh}([\chi_i,\chi_{i+1}]) \cong S_{inc}([\chi_i,\chi_{i+1}])$ for such specimens. This indicates that the area $S_{sm}([\lambda_t(i+1),\lambda_t(i)])$, between each interval $[\lambda_t(i+1),\lambda_t(i)]$ and its respective segment $T_{sm}([\lambda_t(i+1),\lambda_t(i)])$ of $T_{sm}(\lambda)$, should be almost independent of interference pattern shrinkage caused by the partial coherence of the light propagating through the film.

Based on the above, $S_{sm}([\lambda_t(i+1),\lambda_t(i)])$ is approximated as follows by using Eq. (1):

$$S_{sm}([\lambda_t(i+1), \lambda_t(i)]) = \int_{\lambda_t(i+1)}^{\lambda_t(i)} T_{sm}(\lambda)d\lambda \simeq A_1(\lambda) \int_{\lambda_t(i+1)}^{\lambda_t(i)} x_c(\lambda)d\lambda = A_1(\lambda) \int_{\lambda_t(i+1)}^{\lambda_t(i)} e^{-4\pi k_c \bar{\mathrm{d}}/\lambda} d\lambda$$
$$\simeq A_1(\lambda) \int_{\lambda_t(i+1)}^{\lambda_t(i)} (1 - 4\pi k_c \bar{\mathrm{d}}/\lambda)d\lambda \simeq A_2(\lambda) - A_3(\lambda) \int_{\lambda_t(i+1)}^{\lambda_t(i)} k_c(\lambda)d\lambda \simeq A_2(\lambda) - A_3(\lambda) \int_{\lambda_t(i+1)}^{\lambda_t(i)} k(\lambda)d\lambda\ , \tag{13}$$

where $A_1(\lambda)$, $A_2(\lambda)$, and $A_3(\lambda)$ are known functions almost independent from $k(\lambda)$, and fast changing compared to it. Eq. (13) shows that the two areas between the interval $[\lambda_t(i+1),\lambda_t(i)]$ and its respective $k([\lambda_t(i+1),\lambda_t(i)])$ and $k_c([\lambda_t(i+1),\lambda_t(i)])$ should be almost equal, for each $[\lambda_t(i+1),\lambda_t(i)]$.

Furthermore, the unknown extinction coefficient of the film is expressed as $k[T_{sm}(\lambda)] = k_0(\lambda) + \Delta k(\lambda)$. Notably, predominantly coherent light propagates through the film, with a small incoherent light component mostly due to the roughness of the air/film surface and the slit width, and $k_0(\lambda)$ represents the coherent light approximation of $k[T_{sm}(\lambda)]$. Therefore, $\Delta k(\lambda)$ represents a partially coherent light correction of $k_0(\lambda)$.

Since both $k(\lambda)$ and $k_0(\lambda)$ are smooth functions without small humps, $\Delta k(\lambda)$ should be also a smooth function without small humps. In this regard, using Eq. (13) leads to the following formula for $\Delta k(\lambda)$:

$$\int_{\lambda_t(i+1)}^{\lambda_t(i)} \Delta k(\lambda)d\lambda = \int_{\lambda_t(i+1)}^{\lambda_t(i)} [k(\lambda) - k_0(\lambda)]d\lambda \simeq \int_{\lambda_t(i+1)}^{\lambda_t(i)} [k_c(\lambda) - k_0(\lambda)]d\lambda = \int_{\lambda_t(i+1)}^{\lambda_t(i)} [\Delta k_+(\lambda) + \Delta k_-(\lambda)]/2d\lambda \rightarrow$$
$$\rightarrow \Delta k(\lambda) \simeq [\Delta k_+(\lambda) + \Delta k_-(\lambda)]/2, \tag{14}$$

where $\Delta k_+(\lambda)$ and $\Delta k_-(\lambda)$ are envelopes of the difference $k_c(\lambda)$-$k_0(\lambda)$. $\Delta k_+(\lambda)$ and $\Delta k_-(\lambda)$ are respectively obtained by PCHP interpolation over the maxima and the minima of the difference $k_c(\lambda)$-$k_0(\lambda)$, separated by a specified minimum amount. Based on the above, the computation of $\Delta k(\lambda)$ from Eq. (14) provides the extinction coefficient $k(\lambda)$ of the film, determined from $T_{sm}(\lambda)$, as $k[T_{sm}(\lambda)] = k_0(\lambda) + \Delta k(\lambda)$.

Alternatively, $k(\lambda)$ can be computed from $T_+(\lambda)$, e.g. by solution of its approximation from Eq. (5), for each λ. Furthermore, more accurate formula for $T_+(\lambda)$ is derived from Eq. (1) by rewriting

$$\varphi = 4\pi n[\bar{\mathrm{d}} + (d - \bar{\mathrm{d}})]/\lambda = 4\pi n(\bar{\mathrm{d}} + \delta\mathrm{d})/\lambda \xrightarrow[from\ Eq.(2)]{for T_+(\lambda)} \text{which leads to:}$$
$$= 2\pi.\ integer + 4\pi n\delta\mathrm{d}/\lambda,$$

$$T_+(\lambda) = \frac{1}{\varphi_{2_+} - \varphi_{1_+}} \int_{\varphi_{1+}}^{\varphi_{2+}} \mathrm{d}T_u(\varphi_+) = \frac{(\tau_{a,f}\tau_{f,s}\tau_{s,a})^2 x_s}{\varphi_{2_+} - \varphi_{1_+}} \int_{\varphi_{1+}}^{\varphi_{2+}} \frac{x d\varphi_+}{a_1 - b_1\cos(\varphi_+) + c_1\sin(\varphi_+)}, \tag{15}$$

where $\varphi_+ = 4\pi n(\delta d)/\lambda$, $\varphi_{1_+} = -4\pi n\Delta\mathrm{d}/\lambda$, $\varphi_{2_+} = 4\pi n\Delta\mathrm{d}/\lambda$.

3. Results

The algorithm from Fig. 2 is used for characterization of the a-Si films from the specimens A041 and A038, and the obtained results are reported in this Section. The substrate absorbance $x_s(\lambda)$, $T(\lambda)$, the envelopes $T_+(\lambda)$ and $T_-(\lambda)$, and the adjusted $T_+(\lambda_{t-})$ and $T_-(\lambda_{t+})$ calculated from Eqs. (8,9) in the region with $x_s(\lambda) < 1$ are presented in Fig. 3 for the specimens A038 and A041. $T_{sm}(\lambda)$ is based on 'internal smoothing' only in the region λ = [1770,2350] nm of $T(\lambda)$ for the specimen A038, as seen from the inset of Fig. 3b, due to absorption by CO_2 and water vapor traces revealed by ragged looking $\mathrm{d}T/\mathrm{d}\lambda$ in this region [12].

First stage characterizations are performed of the films A038 and A041 in both cases of the points $T_+(\lambda_{t-})$ and $T_-(\lambda_{t+})$, respectively, being non-adjusted and adjusted in the region $x_s(\lambda) < 1$. The obtained results are exhibited in Table 1.

According to [5], the computed results for $\bar{\mathrm{d}}$, $\Delta\mathrm{d}$, and m_1, from first stage characterization by the OEM of a particular specimen, correspond to the smallest value of the error metric SD/N. Therefore, the results from the first stage characterizations are $\bar{\mathrm{d}}$ = 3929.9 nm, $\Delta\mathrm{d}$ = 53.5 nm, m_1 = 12 for the film A041, and $\bar{\mathrm{d}}$ = 774.6 nm, $\Delta\mathrm{d}$ = 26.7 nm, m_1 = 2 for the film A038.

Second stage characterizations of the films A038 and A041 are performed employing the above values of their parameters $\bar{\mathrm{d}}$, $\Delta\mathrm{d}$, and m_1. Approximated values $n_0\{\lambda_t,\lambda_a\}$ of the refractive index are calculated from Eq. (2), and the refractive index $n(\lambda)$ of the film is determined by curve fitting over $n_0\{\lambda_t,\lambda_a\}$. For the film A041, the fitting function over $n_0\{\lambda_t,\lambda_a\}$ is a polynomial of optimized degree 5 obtained from Eq. (10); and the fitting function is a two-term exponential, defined in Eq. (10), for the film A038.

The rough estimate $k_c(\lambda)$ of the extinction coefficient of the film is computed from Eq. (1) using the known $T_{sm}(\lambda)$, and the approximation $k_0(\lambda)$ of the extinction coefficient is determined by curve fitting over $k_c\{\lambda_t,\lambda_a\}$. For the film A041, the fitting function over $k_c\{\lambda_t,\lambda_a\}$ is a polynomial of optimized degree 8 obtained from Eq. (10). For the film A038, two different two-term exponential fitting functions are employed below and above $\lambda_t(4)$ = 1429 nm, and $k_c[\lambda_t(2)$ = 1969 nm] is not used in the curve fitting. The obtained results related to $n(\lambda)$ of the

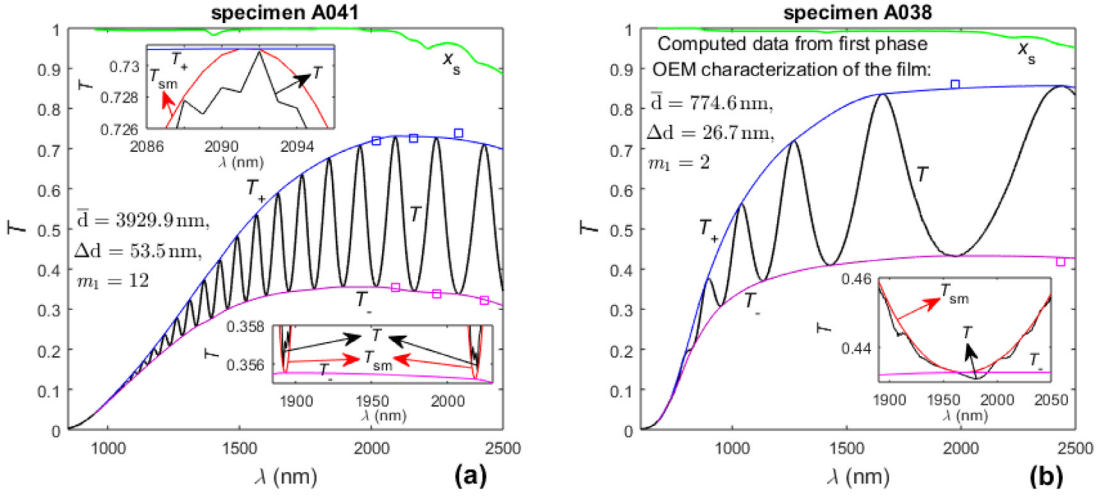

Figure 3. a) and b) Normal incidence transmittance $T(\lambda)$, the envelopes $T_+(\lambda)$ and $T_-(\lambda)$, and $x_s(\lambda)$ for the specimens A041 and A038. In the insets are shown magnified images including $T_{sm}(\lambda)$ obtained by 'external smoothing' of $T(\lambda)$ and slit width correction, unlike in [3–5]. The adjusted points $T_+(\lambda_{t-})$ and $T_-(\lambda_{t+})$ in the region with $x_s(\lambda) < 1$ are displayed by squares.

Table 1
Results from first stage characterizations of the films A038 and A041 based on the algorithm from Fig. 2. The data for $\bar{d}$, Δd, and m_1 corresponding to the smaller value of the error metric *SD*/N represent the computed values of these parameters and are displayed in red. The respective results obtained in [12] are in blue.

first stage characterizations			
based on the algorithm from Fig. 2			
Case Study (C)	$T_+(\lambda_{ti-})$ & $T_-(\lambda_{ti+})$	Value of the error metric: *SD*/N (nm) or *RSMD*/N	Results: $\bar{d}$ (nm), Δd (nm), m_1
film A041			
C41a	are Adjusted in the region	*SD*/N = 0.567 nm	**3929.9 nm, 53.5 nm, 12**
C41b	$x_s(\lambda)<1$	*RSMD*/N = 2.11×10^{-3}	3932.6 nm, 53.4 nm, 12
C41c	are not Adjusted in the region	*SD*/N = 0.592 nm	3949.8 nm, 52.8 nm, 12
C41d	$x_s(\lambda)<1$	*RSMD*/N = 2.45×10^{-3}	3953.0 nm, 52.7 nm, 12
*	best result from [12]	*SD*/N = 0.594 nm	**3939.1 nm, 53.1 nm, 12**
film A038			
C38a	are adjusted in the region	*SD*/N = 0.318 nm	**774.6 nm, 26.7 nm, 2**
C38b	$x_s(\lambda)<1$	*RSMD*/N = 1.42×10^{-3}	773.8 nm, 26.9 nm, 2
C38c	are not Adjusted i n the region	*SD*/N = 0.453 nm	783.1 nm, 24.4 nm, 2
C38d	$x_s(\lambda)<1$	*RSMD*/N = 1.77×10^{-3}	781.9 nm, 24.7 nm, 2
*	best result from [12]	*SD*/N = 0.341 nm	**785.7 nm, 23.1 nm, 2**

films A038 and A041 are shown in Fig. 4a, and these related to $k_0(\lambda)$ - in Figs. 4b and 4c. The significantly lower values of $n(\lambda)$ of the film A038 compared to the film A041, as seen from Fig. 4a, are consistent with our recent results for similarly prepared a-Si films, which showed that $n(\lambda)$ decreases with increasing the Ar pressure [20].

Regarding the characterization of the film A038, it is seen from the inset of Fig. 3b and Fig. 4 that the not used in the curve fitting point k_c [$\lambda_t(2)$ = 1969 nm] is in the region λ = [1770,2350] nm influenced by residual CO_2 and water vapor absorption. The reason for the too low value of $k_c[\lambda_t(2)]$ is that the 'internal smoothing' of $T(\lambda)$, performed only in this region, has provided too low $T_{sm}[\lambda_t(2)]$; leading to little higher $n[\lambda_t(2)]$ and quite lower $k_c[\lambda_t(2)]$, since in this region $T_{sm}(\lambda) \sim (\tau_{a,f}\,\tau_{f,s})^2 x \sim (n^2 + k_c^2).1$. Moreover, the data from Fig 4 and Table 2 reveal that best curve fitting of $n_0\{\Lambda_f\}$ and $k_c\{\Lambda_f\}$ is obtained employing respectively 1 and 2 'two-term exponent' from Eq. 10. Besides, the results from Table 2 show that using $k[T_{sm}(\lambda)]$ provides lower accuracy film characterization than using $k[T_+(\lambda)]$. This is attributed to the absorption in the region λ = [1770,2350] nm influenced by residual CO_2 and water vapor, which has led to too low $T_{sm}[\lambda_t(2)]$; while not changing any $T_+[\lambda_t(i)]$ since there is no maximum of $T_{sm}(\lambda)$ in this region.

The difference $k_c(\lambda)$ - $k_0(\lambda)$, the envelopes $\Delta k_+(\lambda)$ and $\Delta k_-(\lambda)$ obtained by PCHPI over its maxima and minima, and the correction $\Delta k(\lambda) = [\Delta k_+(\lambda) + \Delta k_-(\lambda)]/2$ of $k_0(\lambda)$ are drawn in Fig. 5a for the film A041. The spectral dependencies of $k_0(\lambda)$, $k[T_{sm}(\lambda)] = k_0(\lambda) + \Delta k(\lambda)$, and $k[T_+(\lambda)]$ computed by solving Eq. (15) are shown in Figs. 5a and 5b for the films A041 and A038.

Reconstructed transmittance spectra $T_r(\lambda)$ are computed by replacing $\bar{d}$, Δd, $n(\lambda)$ and $k(\lambda)$ in the right side of Eq. (1). Spectral dependencies T-$T_r(\lambda)$ are presented in Fig. 6.

It is seen from Fig 6b, for the specimen A038, that $T(\lambda)$ is closer to $T_r(\lambda)$ using $k[T_{sm}(\lambda)]$ for $\lambda<\lambda_b$ and closer to $T_r(\lambda)$ using $k[T_+(\lambda)]$ for $\lambda>\lambda_b$, whereas $k[T_{sm}(\lambda_b)] \approx k[T_+(\lambda_b)]$. This indicates that most accurate characterization of the film A038 is achieved employing extinction coefficient $k[T_{sm}(\lambda<\lambda_b)]$ and $k[T_+(\lambda>\lambda_b)]$.

Regarding the selection of the most accurate characterization results for the films A041 and A038, $T_r(\lambda)$ are computed from Eq. (1) for several types of the fitting functions for $n(\lambda)$ and $k_0(\lambda)$, and the employed $k(\lambda)$. Respective figures of merit FOM_1 to FOM_4 are calculated from Eq. (7) and refer to employing four different extinction coefficients: $k[T_{sm}(\lambda)] = k_0(\lambda) + \Delta k(\lambda)$, $k_0(\lambda)$, $k[T_+(\lambda)]$, as well as $k[T_{sm}(\lambda<\lambda_b)]$ and $k[T_+(\lambda>\lambda_b)]$. The values of FOM_1 to FOM_4 are presented in Table 2 depending on the features of the performed characterizations.

The results with lowest *FOM* for the film A041, displayed in red in Table 2, confirm that its $n(\lambda)$ and $k_0(\lambda)$ are best represented by curve fitting over $n_0\{\Lambda_f\}$ and $k_c\{\Lambda_f\}$ with polynomials of optimized degrees of 5 and 8, respectively, and employing $k[T_{sm}(\lambda)] = k_0(\lambda) + \Delta k(\lambda)$. It is also seen from Table 2 that $n(\lambda)$ and $k_0(\lambda)$ of the film A038 are best represented by curve fitting over $n_0\{\Lambda_f\}$ and $k_c\{\Lambda_f\}$ with one and two different 'two-term exponent', as described in Fig. 4, employing $k[T_{sm}(\lambda<1600nm)] = k_0(\lambda) + \Delta k(\lambda)$ and $k[T_+(\lambda>1600nm)]$.

The Wemple-DiDomenico approximation (WDA) $n(E) \simeq \sqrt{1 + \frac{E_0 E_d}{[E_0^2 - E^2(\lambda)]}}$ is known to be valid for amorphous

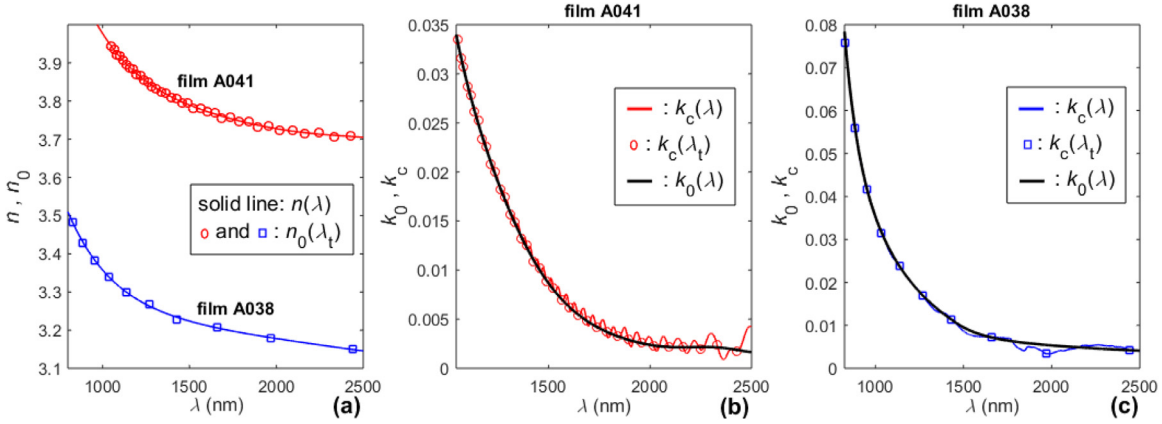

Figure 4. Spectral characteristics related to $n(\lambda)$ and $k_0(\lambda)$ of the films A041 and A038. a) $n(\lambda)$ determined by curve fitting to $n_0\{\Lambda_f\}$. b) and c) $k_c[T_{sm}(\lambda)]$ and $k_0(\lambda)$ determined by curve fitting to $k_c\{\Lambda_f\}$.

Table 2
Results from second stage characterizations of the films A041 and A038 based on the algorithm from Fig. 2. The figures of merit FOM_1, FOM_2 and FOM_3 are calculated from Eq. (7), whereas $T_r(\lambda)$ is computed from Eq. (1). The lowest *FOM*s are displayed in red. The respective results from [6] are in blue.

second stage characterizations based on the algorithm from Fig. 2						
Input results from (C)	Case Study	Features	FOM_1 for $k=k_0+\Delta k$	FOM_2 for $k=k_0$	FOM_3 for k from T_+	FOM_4 for $k(\lambda<\lambda_b)=k_0+\Delta k$, $k(\lambda\geq\lambda_b)$ from T_+
film A041						
C41a	C41aa	$n_0\{\Lambda_f\}$, $k_c\{\Lambda_f\}$ are fit by polynomials of optimized degrees of 5 and 8. FOM_3 uses k, and T_+ from Eq. (15).	**5.71×10^{-3}**	7.39×10^{-3}	7.78×10^{-3}	
C41a	C41ab	$n_0\{\Lambda_f\}$ is fit by polynomial of 4-th degree, and $k_c\{\Lambda_f\}$ - by 2 'two-term exponent'. FOM_3 uses k, Eq. (15).	5.75×10^{-3}	7.36×10^{-3}	7.78×10^{-3}	
C41a best	C41ac	$n_0\{\Lambda_f\}$, $k_c\{\Lambda_f\}$ are fit by polynomials of optimized degrees of 5 and 8. FOM_3 uses k, and T_+ from Eq. (5). $\bar{d}=3939.1$nm, $\Delta d=53.1$nm, $m_1=12$.	5.71×10^{-3}	7.39×10^{-3}	7.78×10^{-3}	
result in [12]	C41ad	Small humps in both $n(\lambda)$ and $k_0(\lambda)$ obtained by PCHP interpolation.		**6.99×10^{-3}**		
film A038						
C38a	C38aa	$n_0\{\Lambda_f\}$ and $k_c\{\Lambda_f\}$ are fit by 1 and 2 'two-term exponent'. FOM_3 uses k, and T_+ from Eq. (15).	3.03×10^{-3}	2.17×10^{-3}	2.08×10^{-3}	**1.89×10^{-3} for $\lambda_b\approx1600$ nm**
C38a	C38ab	$n_0\{\Lambda_f\}$ is fit by polynomial of 5-th degree, and $k_c\{\Lambda_f\}$ by 2 'two-term exponent'. FOM_3 uses k, Eq. (15).	There is no optimized degree polynomial fit of $n_0(\lambda_t)$, and the fit of $k_c\{\Lambda_f\}$ contains humps.			
C38a best	C38ac	$n_0\{\Lambda_f\}$ and $k_c\{\Lambda_f\}$ are fit by 1 and 2 'two-term exponent'. FOM_3 uses k, and T_+ from Eq. (5). $\bar{d}=785.0$ nm, $\Delta d=23.5$ nm, $m_1=2$.	3.03×10^{-3}	2.17×10^{-3}	2.07×10^{-3}	
result in [12]	C38ad	Small humps in both $n(\lambda)$ and $k_0(\lambda)$ obtained by PCHP interpolation.		**2.63×10^{-3}**		

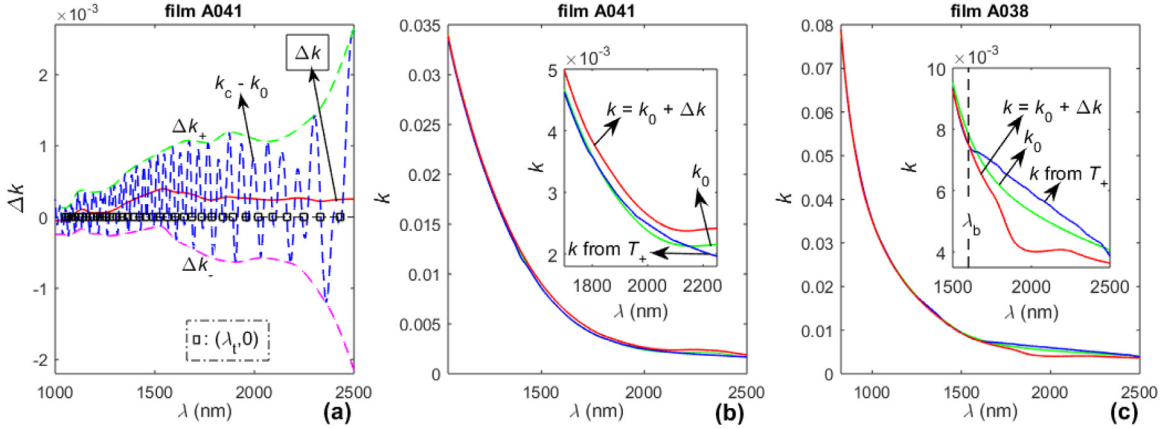

Figure 5. Spectral characteristics related to $k(\lambda)$. a) The correction $\Delta k(\lambda)=[\Delta k_+(\lambda)+\Delta k_-(\lambda)]/2$, where $\Delta k_+(\lambda)$ and $\Delta k_-(\lambda)$ are envelopes of the difference $k_c(\lambda)$ - $k_0(\lambda)$, for the A041 film. b) and c) $k_0(\lambda)$, $k[T_{sm}(\lambda)] = k_0(\lambda) + \Delta k(\lambda)$, and $k[T_+(\lambda)]$ computed by solving Eq. (15), for the A041 and A038 films.

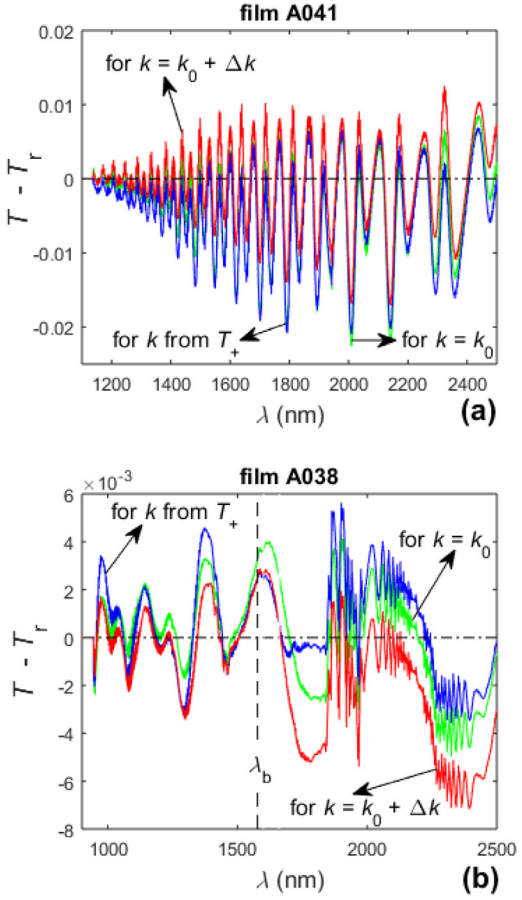

Figure 6. Spectral dependencies T-$T_r(\lambda)$ for the film characterizations providing refractive index $n(\lambda)$ and extinction coefficient either $k[T_{sm}(\lambda)] = k_0(\lambda) + \Delta k(\lambda)$, $k_0(\lambda)$, or $k[T_+(\lambda)]$. a) for the specimen A041. b) for the specimen A038; $T(\lambda)$ is closer to $T_r(\lambda)$ using $k[T_{sm}(\lambda < \lambda_b \approx 1600\ \text{nm})]$ and closer to $T_r(\lambda)$ using $k[T_+(\lambda > \lambda_b)]$, whereas $k[T_{sm}(\lambda_b)] \approx k[T_+(\lambda_b)]$.

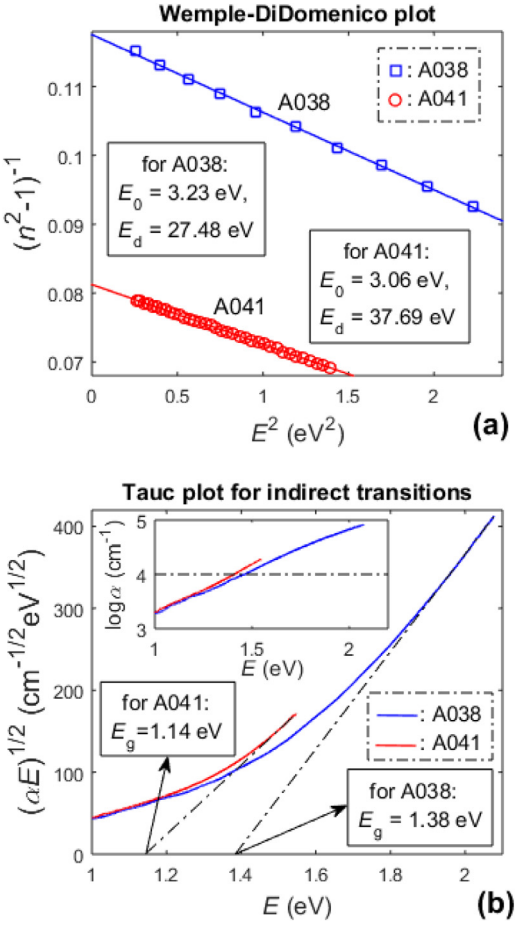

Figure 7. Results for the films A038 and A041 computed by: (a) the Wemple-DiDomenico approximation, (b) the Tauc approximation for indirect electronic transitions.

semiconductors, where $E_0 > E$ is the single-effective-oscillator energy and E_d is the oscillator strength [35]. Therefore, the parameters E_0 and E_d are determined by a linear regression of the WDA dependence $[n(\lambda_t)^2\text{-}1]^{-1}$ versus $E(\lambda_t)^2$; followed by computation of $n(\lambda)$ from the WDA for $\lambda[T(\lambda) \approx 0] < \lambda < \min(\lambda_t)$, its respective $k(\lambda)$ obtained from Eq.(1), and the absorption coefficient $\alpha(\lambda) = 4\pi k(\lambda)/\lambda$ of the film. Furthermore, the Tauc optical gap E_g is obtained using a linear regression of the Tauc approximation $(\alpha E)^{1/2} = B_T(E\text{-}E_g)$ for indirect electronic transitions, whereas $\alpha > 10^4$ cm^{-1} [1]. The results from these computations are shown in Fig. 7.

The Tauc slope B_T is also determined using the linear regression with $\alpha > 10^4$ cm^{-1} of the same Tauc approximation [1]. The Urbach energy E_U, representing the width of the energy range over which $\alpha(E)$ tails off exponentially, is determined by an exponential regression with $\alpha < 10^4$ cm^{-1} of the Urbach approximation $\alpha(E) = \alpha_0 \exp(E/E_U)$ [1]. Correspondingly, it is established that B_T = 423.8 (cm.eV)$^{-1/2}$ and E_U = 235 meV for the film A041, as B_T = 594.4 (cm.eV)$^{-1/2}$ and E_U = 274 meV for the film A038.

SEM image of a cross-section of the film A038 and AFM image of the free surface of the same film are shown in Fig. 8, as our SEM data for $\bar{d}$ have been calibrated by data for $\bar{d}$ from Veeco Dektak 150 mechanical surface profiler [20]. The difference between the average thickness $\bar{d}$ = 774.6 nm of the film A038 obtained from Table 1 and from this SEM image is 0.36 %, thus confirming the accuracy of the first stage film characterization based on the algorithm from Fig. (2).

The RMS surface roughness of the film A038 is $Rq \approx 1.5$ nm, and such roughness spreads over areas of ~ 50 μm × 50 μm on the surface

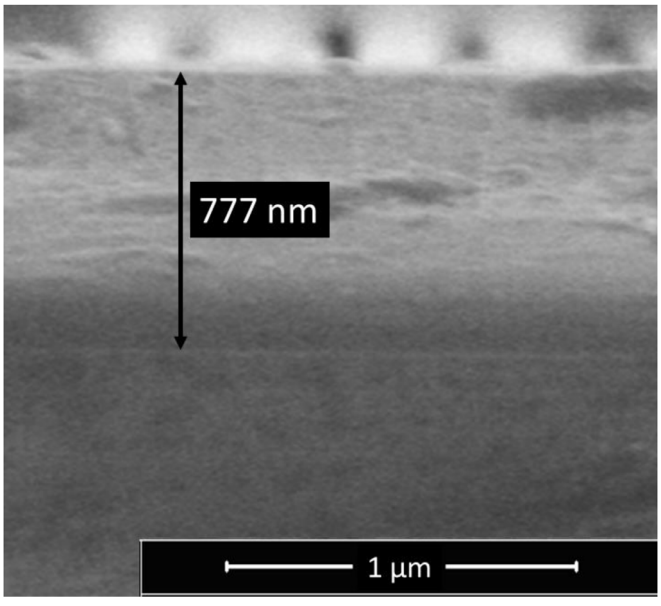

Figure 8. SEM image of a cross-section of the film A038, as the thickness of 777 nm is the value at the arrow location.

film/air. On the other hand, the maximum deviation of the film thickness d from the average thickness $\bar{d}$ over the light spot area of 10 mm × 3 mm on the surface film/air is $\Delta d \approx 26.7$ nm, according to the

result in red from Table 1. In such a case of $Rq << \Delta d << \lambda$, Δd causes a significant shrinkage of $T(\lambda)$ towards the lower λ, whereas the film surface roughness induces noise in $T(\lambda)$ and its slight shrinkage, as illustrated in Fig. 1b.

4. Discussion

The *FOM* based comparative study [12] of characterization of the A041 and A038 films, by the OEM [5], OGM [23], and the most relevant spectroscopic ellipsometry related methods TLUM [24] and CLUM [25], showed that the OEM provided most accurate characterization of both films. However, the OEM modification in [12] used envelopes $T_+(\lambda)$ and $T_-(\lambda)$ adjusted for $x_s(\lambda) \leq 1$ whose preparation is ambiguous and difficult, as well as interpolation of $n(\lambda)$ over $n(\lambda_t)$ and of $k(\lambda)$ over $k_t(\lambda_t)$ leading to appearance of spurious small humps in both $n(\lambda)$ and $k(\lambda)$. These facts caused reviewing the OEM modification from [12] to investigate whether these problems can be resolved, and resulted in development of the algorithm for perfecting the EM characterization of a thin film on glass substrate presented in Figure 2. The improvements in the algorithm from Fig. 2 are discussed below with respect to the algorithm of the OEM modification from [12].

The employed here computation of the envelopes $T_+(\lambda)$ and $T_-(\lambda)$ of $T_{sm}(\lambda)$ is advantageous over the respective approaches from [16] and [17]. Indeed, it combines inclusion of extra points for the interpolation of both envelopes, similarly to [16]; with iterations completed at $S_+^{(l)} = 0$ and $S_-^{(l)} = 0$, similarly to [17], and using right 'boundary points' $T_+^{(l)}(\lambda_L)$ and $T_-^{(l)}(\lambda_L)$ changing with the iteration step number l; thus increasing the accuracy of the envelopes.

Notably, in the computation of the envelopes $T_+(\lambda)$ and $T_-(\lambda)$, obtained from Step A2 of the algorithm, is assumed implicitly $x_s(\lambda < \lambda_L) = 1$. In this regard, $T_+(\lambda_{t-})$ and $T_-(\lambda_{t+})$ are used in the first stages of each main EM version [3–5], and they do not belong to $T_{sm}(\lambda)$; therefore proper adjustment of their values in regions with $x_s(\lambda) < 1$ should lead to more accurate EM characterization. Correspondingly, Eqs. (8,9) are derived to provide adjusted $T_+(\lambda_{t-})$ and $T_-(\lambda_{t+})$ in regions with $x_s(\lambda) < 1$.

Results from Table 1, investigating the influence of the adjustment of $T_+(\lambda_{t-})$ and $T_-(\lambda_{t+})$ in the long wavelengths region with $x_s(\lambda) < 1$ show that this adjustment leads to decreasing the value of the preferred error metric *SD*/N [5] by 4.2% for the specimen A041 and by 29.8% for A038. This demonstrates that the adjustment of $T_+(\lambda_{t-})$ and $T_-(\lambda_{t+})$ in the region with $x_s(\lambda) < 1$ results in increasing the accuracy of OEM based first stage characterization of both films A041 and A038. It is also seen from Table 1 that the use of $T_+(\lambda_{t-})$ and $T_-(\lambda_{t+})$ computed from Eqs. (8,9) in the region with $x_s(\lambda) < 1$ leads to smaller *SD*/N than its respective from [12], and correspondingly results in more accurate first stage characterizations than in [12] for both films A041 and A038. The excellence of the first stage characterizations of the films A041 and A038, employing adjusted $T_+(\lambda_{t-})$ and $T_-(\lambda_{t+})$ in the region with $x_s(\lambda) < 1$, is confirmed by the not exceeding 0.11% difference between the values of $\bar{d}$ from Table 1 obtained by using the error metrics *SD*/N and *RSMD*/N [5].

As already mentioned, the interpolation of $n(\lambda)$ over $n_0[\lambda_t(i)]$ in [12] can lead to appearance of spurious small humps in both $n(\lambda)$ and $k(\lambda)$, due to inevitable small inaccuracies of some $\lambda_t(i)$. Contrarily, the curve fitting over $n_0\{\Lambda_f\}$ and $k_c\{\Lambda_f\}$, employed at Steps A6 and A7 of the algorithm from Fig. 2, diminishes appearance of spurious small humps in both $n(\lambda)$ and $k(\lambda)$. Notably, the fitting function *Ff* for the set $n_0\{\Lambda_f\}$ or $k_c\{\Lambda_f\}$ should be chosen to provide smallest values of $Fr(\{\Lambda_f\})$ expressed in Eq. (10). Importantly, the curve fitting over $n_0\{\Lambda_f\}$ and $k_c\{\Lambda_f\}$ can preserve large humps in $n(\lambda)$ and $k(\lambda)$ inherent to the film material, thus preserving the EM essence of not employing any dispersion model.

To understand the influence of the partial coherence of light propagating through the film on results from film characterization by the algorithm from Fig. 2, it should be taken into account that this algorithm is based on using Eqs. (1,2) assuming propagation of coherent light through the film. In this regard, the film characteristics $\bar{d}$, Δd, m_1, and $n(\lambda)$ are determined mostly from the wavelengths of the set $\{\lambda_t,\lambda_a\}$ [3–5,12] which are almost independent from the partial coherence of light in the film according to the comments from Steps A1-A3. Furthermore, since $k(\lambda)$ is computed by using Eq. (1) assuming coherent light in film, and $T_{sm}(\lambda)$ influenced by the partial coherence of light in the film, $k(\lambda)$ represents a 'coherent light in film' estimation of the true extinction coefficient affected by the partial coherence of light in the film. However, optical designs including thin films with unintended surface roughness usually employ 'coherent light in film' characteristics; considering monochromatic light in the film, reflected only from its surfaces, to be coherent [1,29,36]. This exemplifies the advantage of using the 'coherent light in film' estimation $k(\lambda)$ of the true extinction coefficient affected by the partial coherence of light in the film, associated with light scattering from the film.

According to [12], the most accurate film characterization over the wavelengths interval $[\min(\lambda_t),\lambda_t(1)]$ is identified by its smallest *FOM* computed from Eq. (7). Correspondingly, the data displayed in red in Table 2 indicate that the most accurate film characterization of the film A041 is achieved using curve fitting of $n_0\{\Lambda_f\}$ and $k_c\{\Lambda_f\}$ by polynomials of respective optimized degrees of 5 and 8, as described in Eq. (10), and $k[T_{sm}(\lambda)] = k_0(\lambda) + \Delta k(\lambda)$. Moreover, it is seen from Fig. 5a that $\Delta k(\lambda \subset [1500,2500]\ \text{nm}) = [0.00025,0.0004]$. To explain the obtained $\Delta k(\lambda) > 0$, it is taken into account that the algorithm for film characterization from Fig. 2 is based on Eq. (1), valid for propagation of coherent light through the film, which provides the average film thickness $\bar{d}$ and the coherent light approximation $k_0(\lambda)$ of $k(\lambda)$. Moreover, the influence of $k_0(\lambda)$ on $T_{sm}(\lambda)$ from Eq. (1) is determined by the absorbance $x_0(\lambda) = \exp(-4\pi k_0\bar{d}/\lambda)$, and therefore is dominated by the product $k_0\bar{d}$ for a given wavelength λ. However, a light ray scattered at the surface air/film, propagates over a distance $d > \bar{d}$ in the film; and its dominating product $k_0 d$ is perceived by Eq. (1) as $(k_0 + \Delta k)\bar{d} = k_0 d$, where $\Delta k > 0$ is partially coherent light correction of the extinction coefficient due to the light scattering.

Data displayed in red in Table 2 confirm that lowest $FOM \approx 1.89\times10^{-3}$ for the film A038, representing its most accurate characterization, is achieved using $k[T_+(\lambda > \lambda_b)]$ and $k[T_{sm}(\lambda < \lambda_b)]$. Considering the distortion of $T(\lambda)$ of the specimen A038 in the region $\lambda = [1770,2350]$, associated with residual gas absorption, this very low value of *FOM* shows that accurate film characterization can be achieved by using the algorithm from Fig. 2 even when $T(\lambda)$ is influenced by residual gas absorption. Furthermore, taking into account data from [12], $FOM \approx 1.89\times10^{-3}$ for the film A038 from Table 2 represents a record low value of *FOM*.

Notably, the results for FOM_3 from Table 2 indicate that there is practically no difference in the accuracy of characterization, of either of the films A041 and A038, performed using Eq. (5) or the more precise Eq. (15) for computation of $k[T_+(\lambda)]$. Importantly, however, the *FOM* data displayed in red and blue in Table 2 show that the lowest *FOM*s in this study are 18.3% lower for the film A041 and 28.1% lower for the film A038 compared with the respective lowest *FOM*s for the same films from [12]. This result and the absence of spurious small humps in $n(\lambda)$ and $k(\lambda)$ presented in Figs. (4a), (5b) and (5c), unlike the presence of such humps in $n(\lambda)$ and $k(\lambda)$ from [12], demonstrate the significantly higher accuracy of characterization of the films A041 and A038 achieved here compared to [12].

5. Conclusions

In this study is proposed an algorithm for perfecting the thin film characterization, based on the optimizing envelope method OEM, without employing a dispersion model. It is shown that this algorithm provides $n(\lambda)$ and $k(\lambda)$ without spurious small humps, more accurate characterization of the films A041 and A038 than the characterizations of these films from [12], and a record low value of *FOM*.

These results indicate that the proposed algorithm has a capacity for providing most accurate characterization of almost every dielectric or semiconductor film with $\bar{d}$ = [300,5000] nm on a substrate, only from the normal incidence $T(\lambda)$, compared to all the other methods for characterization of such films only from $T(\lambda)$. Our group intends to develop software for characterization of a variety of thin films, based on this algorithm.

Acknowledgments

This work was supported by the European Regional Development Fund within the Operational Programme "Science and Education for Smart Growth 2014-2020" under the Project CoE "National Center of Mechatronics and Clean Technologies", Contract No. BG05M2OP001-1.001-0008, L10S7 SynChaLab.

References

[1] O. Stenzel, The physics of thin film optical spectra, Springer Series in Surface Sciences, Heidelberg (2016).
[2] E. Marquez, A.M. Bernal-Oliva, J.M. Gonzalez-Leal, R.P. Alcon, J.C. Navarro, D. Minkov, Optical constants in the subgap region and vibrational behavior by far-infrared spectroscopy of wedge-shaped obliquely-deposited amorphous GeS_2 films, Phys. Scripta 60 (1999) 90–96.
[3] R. Swanepoel, Determination of the thickness and optical constants of amorphous silicon J, Phys. E: Sci. Instrum. 16 (1983) 1214–1222.
[4] J.M.G. Leal, R.P. Alcon, J.A. Angel, D.A. Minkov, E. Marquez, Influence of substrate absorption on the optical and geometrical characterization of thin dielectric films, Appl. Opt. 41 (2002) 7300–7308.
[5] D.A. Minkov, G.M. Gavrilov, G.V. Angelov, G.M.D. Moreno, C.G. Vazquez, S.M.F. Ruano, E. Marquez, Optimisation of the envelope method for characterisation of optical thin film on substrate specimens from their normal incidence transmittance spectrum, Thin Solid Films 645 (2018) 370–378.
[6] S.C Chiao, B.G. Bovard, H.A. Macleod, Optical-constant calculation over an extended spectral region: application to titanium dioxide film, Appl. Opt. 34 (1995) 7355–7359.
[7] J.S. Gonzalez, A.D. Parralejo, A.L. Ortiz, F. Guiberteau, Determination of optical properties in nanostructured thin films using the Swanepoel method, Appl. Surf. Sci 252 (2006) 6013–6017.
[8] L. Gao, F. Lemarchand, M. Lequime, Refractive index determination of SiO2 layer in the UV/Vis/NIR range: spectrophotometric reverse engineering on single and bi-layer designs, J. Europ. Opt. Soc. Rap. Public. 8 (2013) 13010 1-8.
[9] S.T. Yen, P.K. Chung, Extraction of optical constants from maxima of fringing reflectance spectra, Appl. Opt 54 (2015) 663–668.
[10] Y. Jin, B. Song, Z. Jia, Y. Zhang, C. Lin, X. Wang, S. Dai, Improvement of Swanepoel method for deriving the thickness and the optical properties of chalcogenide thin films, Opt. Express 25 (2017) 440–451.
[11] Y. Jin, B. Song, C. Lin, P. Zhang, S. Dai, T. Xu, Q. Nie, Extension of the Swanepoel method for obtaining the refractive index of chalcogenide thin films accurately at an arbitrary wavenumber, Opt. Express 25 (2017) 31273–31280.
[12] D.A. Minkov, G.V. Angelov, R.N. Nestorov, E. Marquez, E. Blanco, J.J. Ruiz-Perez, Comparative study of the accuracy of characterization of thin films a-Si on glass substrates from their interference normal incidence transmittance spectrum by the Tauc-Lorentz-Urbach, the Cody-Lorentz-Urbach, the optimized envelopes and the optimized graphical methods, Mater. Res. Express 6 (2019) 03640:1-15.
[13] D. Poelman, P.J. Smet, Methods for the determination of the optical constants of thin films from single transmission measurements: a critical review, J, Phys. D 36 (2003) 1850–1857.
[14] A.E. Bartz, Basic Statistical Concepts, fourth ed., Prentice-Hall Inc., Upper Saddle River, 1999.
[15] D. Minkov, DSc thesis: Characterization of thin films and surface cracks by electromagnetic methods and technologies, Technical University, Sofia (2018).
[16] G.M. Gavrilov, D.A. Minkov, S.M.F.Ruano E.Marquez, Advanced computer drawing envelopes of transmittance spectra of thin film specimens, Int. J. Adv. Res. Sci. Eng. Technol 3 (2016) 163–168.
[17] M. McClain, A. Feldman, D. Kahaner, X. Ying, An algorithm and computer program for the calculation of envelope curves, Comput. Phys 5 (1991) 45–48.
[18] Esco Optics, Inc., catalog, materials-fused-silica-quartz.
[19] E. Gaudet, J. Desforges, S. Gauvin, New developments in the determination of the complex refractive index of arbitrary absorptance thin films from envelope profiles of a single transmittance curve, Proc. SPIE 10528, Optical Components and Materials XV 105281H (2018), https://doi.org/10.1117/12.2287933.
[20] E. Márquez, E. Saugar, J.M. Díaz, C. García-Vázquez, S.M. Fernández-Ruano, E. Blanco, J.J. Ruiz-Pérez, D.A. Minkov, The influence of Ar pressure on the structure and optical properties of non-hydrogenated a-Si thin films grown by rf magnetron sputtering onto room temperature glass substrates, J, Non-Cryst. Solids 517 (2019) 32–43.
[21] K.A. Stewart, B.S. Yeh, J.F. Wager, Amorphous semiconductor mobility limits. J. Non-Cryst, Solids 432B (2015) 196–199.
[22] M. Foldyna, K. Postava, J. Bouchala, J. Pistora, T. Yamaguchi, Model dielectric functional of amorphous materials including Urbach tail, Proc SPIE 5445 (2004) 301–305.
[23] D.A. Minkov, G.M. Gavrilov, J.M.D. Moreno, C.G. Vazquez, E. Marquez, Optimization of the graphical method of Swanepoel for characterization of thin film on substrate specimens from their transmittance spectrum, Meas. Sci. Technol., Meas. Sci. Technol 28 (2017) 035202.
[24] L.V.R. DeMarcos, J.I. Larruquert, Analytic optical-constant model derived from Tauc-Lorentz and Urbach tail, Opt. Express 24 (2016) 28561:1-12.
[25] A.S. Ferlauto, G.M. Ferreira, J.M. Pearce, C.R. Wronski, R.W. Collins, X. Deng, G. Ganguly, Analytical model for the optical functions of amorphous semiconductors from the near-infrared to ultraviolet: Applications in thin film photovoltaics, J. Appl. Phys. 92 (2002) 2424–2436.
[26] F.N. Fritsch, R.E Carlson, Monotone piecewise cubic interpolation, SIAM J. Numer. Anal 17 (1980) 238–246.
[27] D. Minkov, Method for determining the optical constants of a thin film on a transparent substrate, J. Phys. D. 22 (1989) 199–205.
[28] I. Simonsen, A. Larsen, E. Andreassen, E. Ommundsen, K. Nord-Varhaug, Haze of surface random systems: An approximate analytic approach, Phys. Rev. A 79 (2009) 063813:1-16.
[29] N.A. Stathopoulos, A.Botsialas S.P.Savaidis, Z.C. Ioannidis, D.G. Georgiadou, M. Vasilopoulou, G. Pagiatakis, Reflection and transmission calculations in a multilayer structure with coherent, incoherent, and partially coherent interference, using the transmission line method, Appl. Opt 54 (2015) 1492–1504.
[30] D.Y. Smith, M. Inokuti, W. Karstens, A generalized Cauchy dispersion formula and the refractivity of elemental semiconductors, J, Phys.: Condens. Matter. 13 (2001) 3883–3893.
[31] http://www.horiba.com. Cauchy and related empirical dispersion formulae for transparent materials, Technical note. Spectroscopic ellipsometry TN14.
[32] http://www.horiba.com. New amorphous dispersion formula, Technical note. Spectroscopic ellipsometry TN12.
[33] A. Kaw, C. Nguyen, Textbook notes on nonlinear regression, Chapter 5.02, https://nm.mathforcollege.com/chapter-05.02-direct-method/.
[34] D. Minkov, R. Swanepoel, A comparative study of the use of the matrix approach and the flow graph approach for optical analysis of isotropic stratified planar structures, Proc. SPIE. 2540 (1995) 131–138.
[35] S.H. Wemple, Refractive-index behavior of amorphous semiconductors and glasses, Phys. Rev. B. 7 (1973) 3767–3777.
[36] O. Stenzel, Optical coatings: Material aspects in theory and practice, Springer Series in Surface Sciences, Heidelberg (2016).